Journal of Solid State Chemistry **166,** 251–258 (2002)
doi:10.1006/jssc.2002.9599, available online at http://www/idealibrary.com on IDEAL®

# Low-Temperature Magnetic Properties of $LuBaCuFeO_{5+\delta}$ and $TmBaCuFeO_{5+\delta}$

A. W. Mombrú,*[,1] A. E. Goeta,† H. Pardo,* P. N. Lisboa-Filho,‡ L. Suescun,* R. A. Mariezcurrena,* O. N. Ventura,§ R. Behak,* K. H. Andersen,‖ and F. M. Araújo-Moreira¶

*Laboratorio de Cristalografía y Química del Estado Sólido, Cátedra de Física, DEQUIFIM, Facultad de Química, Universidad de la República, P.O. Box 1157, Montevideo, Uruguay; †Chemistry Department, University of Durham, Durham DH1 3LE, UK; ‡Laboratorio Interdisciplinar de Eletroquímica e Cerâmicas-LIEC, Departamento de Química, Universidade Federal de São Carlos, São Carlos-SP 13565-905, Brazil; §Computational Chemical-Physics Group, DEQUIFIM, Facultad de Química, Universidad de la República, Montevideo, Uruguay; ‖ISIS, Rutherford-Appleton Laboratories, Chilton, Didcot, Oxon OX11 0QX, United Kingdom; and ¶Departamento de Física, Universidade Federal de São Carlos, São Carlos-SP 13565-905, Brazil

Received January 2, 2002; received in revised form March 19, 2002; accepted March 22, 2002

**The crystal and magnetic structures of the perovskites $LuBaCuFeO_{5+\delta}$ and $TmBaCuFeO_{5+\delta}$ have been studied in the temperature range 2–170 K by neutron powder diffraction. The best fit using the Rietveld method is obtained for the acentric tetragonal space group *P4mm*, with lattice constants $a = 3.774(1)$ Å, $c = 7.474(2)$ Å and $a = 3.7812(2)$ Å, $c = 7.4854(4)$ Å, for $LuBaCuFeO_{5+\delta}$ and $TmBaCuFeO_{5+\delta}$, respectively ($T = 2$ K). The lattice parameters of the unit cell of the magnetic structure for these samples are $a_M = 2a$ and $c_M = 2c$, with a magnetic propagation vector $\mathbf{k} = (\frac{1}{2}, \frac{1}{2}, \frac{1}{2})$. A commensurate magnetic superstructure is detected by the presence of satellites surrounding the $(\frac{1}{2}, \frac{1}{2}, \frac{1}{2})$ magnetic peak at $d \sim 5.1$ Å, determined by $c_{Mcomm.} = 8c$. This superstructure could evolve at $T > 170$ K to a distribution of commensurate and even incommensurate superstructures. A transition to a simple antiferromagnetic structure occurs at $T_2 = 303(3)$ K for $LuBaCuFeO_{5+\delta}$. Evidence of a strong spin freezing effect at $T_1 = 14.0(5)$ K is provided through DC-susceptibility measurements.** © 2002 Elsevier Science (USA)

***Key Words:*** **magnetic structure; commensurate superstructure; spin freezing.**

## 1. INTRODUCTION

The crystal and magnetic structures of the perovskite $YBaCuFeO_{5+\delta}$ (YBCFO) have been studied extensively (1–10) due to the structural similarities with the superconducting cuprate $YBa_2Cu_3O_{7-\delta}$, YBCO. While YBCO presents a square pyramid as the coordination polyhedron around the $Cu^{2+}$ ion, YBCFO exhibits two apex-sharing $CuO_5$ and $FeO_5$ square pyramids, as can be seen in Fig. 1. The aim of many studies concerning this cuprate was to determine whether iron and copper ions are fully disordered in the lamellar network adopting the centrosymmetric space group $P4/mmm$ or are ordered in an acentric structure with both ions occupying inequivalent symmetry sites, space group $P4mm$. Some reports claim that the iron and copper cations are mixed in the same layer, based on neutron powder diffraction studies (7, 9). However, other reports support the occupation of separated layers as deduced from the Mössbauer and Raman spectroscopy studies and neutron powder diffraction as well (4–6, 8).

This cuprate exhibits a standard antiferromagnetic order below $T_N = 442$ K. The determination of the magnetic structure was aided by the fact that all the magnetic origin peaks indexed on the basis of the chemical unit cell as $(\frac{h}{2}, \frac{k}{2}, \frac{l}{2})$ with $h, k, l =$ odd. This implied an enlarged magnetic unit cell with $a_M = 2a$ and $c_M = 2c$ and is only consistent with magnetic ordering schemes of both the $CuO_2$ and $FeO_2$ layers along the c-axis of the form $+[+-]-$ and $+[--]+$ (using the labeling scheme introduced in previous reports (7, 8) with the bracket corresponding to the position of the yttrium). According to Rietveld profile refinements the best magnetic structure model for YBCFO in the $P4mm$ structure (8) is $(+[--]+)_{x,y}$ and $(+[+-]-)_z$ (8).

In addition to the antiferromagnetic ordering transition at $T_N = 442$ K, YBCFO exhibits a commensurate–incommensurate magnetic transition at $T_{N'} = 190$ K. Below this temperature, two sets of satellite peaks surround the $(\frac{1}{2}, \frac{1}{2}, \frac{1}{2})$ magnetic peak at $d \approx 5.15$ Å, collapsing into a single set of satellites below 155 K. The magnetic nature of the $(\frac{1}{2}, \frac{1}{2}, \frac{1}{2})^{\pm}$ satellites has been confirmed by polarization analysis (8).

[1] To whom correspondence should be addressed. Fax: +598-2-9241906. E-mail: amombru@bilbo.edu.uy.



0022-4596/02 $35.00

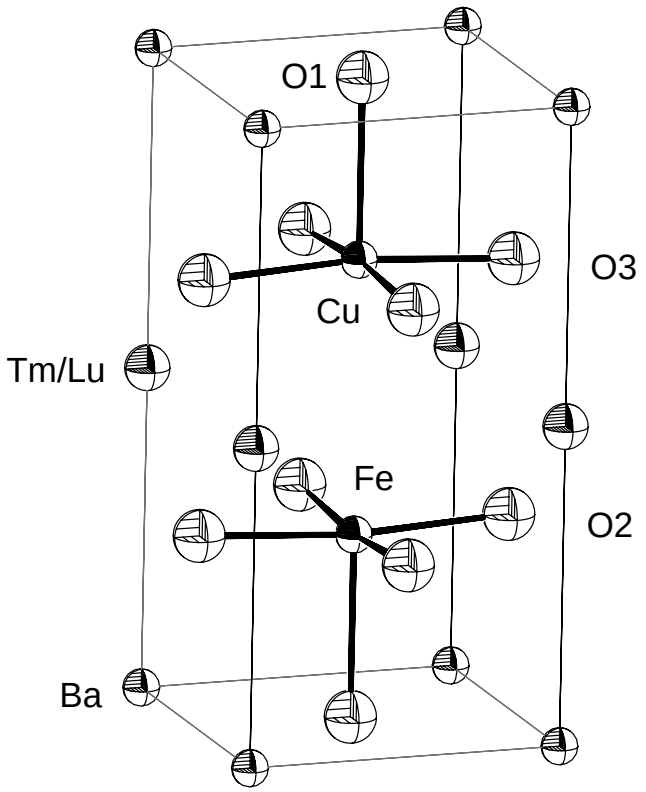


**FIG. 1.** Crystal structure of $REBaCuFeO_{5+\delta}$.

The great importance of YBCO led to the synthesis and structural and physical studies of the *RE*BCO ($REBa_2Cu_3O_{7-\delta}$, *RE*= lanthanides) series. The series of materials obtained by substituting yttrium atoms in the $YBaCuFeO_{5+\delta}$ network by other rare-earth ions, $REBaCuFeO_{5+\delta}$ (*RE*BCFO) have also been studied by the Rietveld analysis from X-ray powder diffraction data and $^{57}Fe$ Mössbauer spectroscopy (11, 12). The data obtained by these techniques provided evidence that the members of this series are isostructural to the tetragonal YBCFO.

The magnetic structures of other members of the *RE*BCFO have been studied and no evidence of any analogous behavior has been found for ions like $Pr^{3+}$ or $La^{3+}$ (13–15). This report presents the low-temperature magnetic structure of two members of the *RE*BCFO series not studied yet (*RE*= Lu, Tm).

## 2. EXPERIMENTAL DETAILS

### 2.1. Sample Preparation

$LuBaCuFeO_{5+\delta}$ (LuBCFO) and $TmBaCuFeO_{5+\delta}$ (TmBCFO) samples were prepared in air by standard solid-state reactions as follows: stoichiometric amounts of $Lu_2O_3$ or $Tm_2O_3$, $BaCO_3$, CuO and $Fe_2O_3$ were fired at 900°C for 24 h; the mixture was then ground and heated at 1000°C for an additional 24 h. Phase purity was established by recording X-ray powder diffraction profiles at room temperature with a Seifert Scintag PADII diffractometer. The homogeneity of the specimens was studied by scanning electron microscopy (SEM) and electron dispersive spectroscopy (EDS) using a Philips XL analytical SEM.

### 2.2. Structural and Magnetic Study

Powder diffraction neutron measurements were performed between 2 and 170 K in the 1.2–7.9 Å *d*-spacing range using the OSIRIS instrument at the ISIS spallation neutron source, Rutherford-Appleton Laboratory, UK.

DC-susceptibility measurements were performed in the temperature range 1.8–400 K (1.8–300 K for TmBCFO), using a Quantum Design MPMS-5 SQUID magnetometer, with applied magnetic fields ($H$) up to 1 T. The DC-susceptibility ($\chi_{DC}$) is presented in emu/g units. Magnetic measurements were taken in two different ways: ZFC (warming after zero-field cooling the sample) and FC (measuring while cooling in an applied magnetic field).

## 3. RESULTS

### 3.1. Microstructural Study

Figure 2 exhibits images of the microstructure of LuBCFO and TmBCFO obtained by scanning electron microscopy showing the homogeneity of the granularity. In order to check the homogeneous distribution of the elements in the specimens, a study using EDS was performed. A composition of images showing the EDS for LuBCFO is exhibited in Fig. 3, where the distribution of Lu, Ba, Cu and Fe is indicated. These figures indicate the good quality of the samples.

### 3.2. Neutron Diffraction Analysis

Rietveld analyses of the neutron diffraction profiles were performed using the GSAS program suite (16), incorporating a pseudo-Voigt function peak shape description and using a cosine Fourier series background.

In view of the earlier structural work on YBCFO (6–9), three structural models were considered: (a) completely disordered structure with the $Fe^{3+}$ and $Cu^{2+}$ ions statistically distributed in the Fe/Cu–$O_2$ layers ($P4/mmm$ space group); (b) fully ordered structure in which the $Fe^{3+}$ and $Cu^{2+}$ ions occupy distinct crystallographic sites ($P4\,mm$ space group) and (c) partially disordered structure in which partial occupation of the $Fe^{3+}$ (or $Cu^{2+}$) site by $Cu^{2+}$ (or $Fe^{3+}$) was allowed ($P4\,mm$ space group). Model (c) was discarded as refinement of the occupancy factor of $Fe^{3+}$ and $Cu^{2+}$ led to the ordered model (b).

The best agreement factors for LuBCFO and TmBCFO were obtained for the refinements using model (b). The

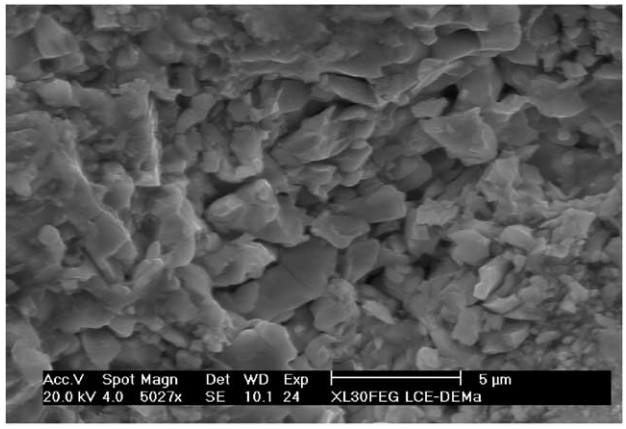


Lu

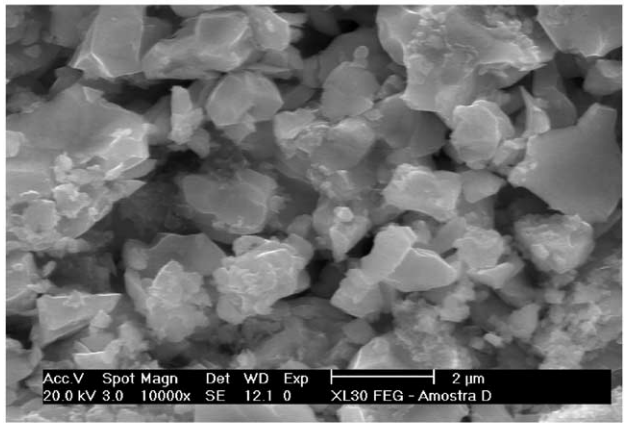


Tm

**FIG. 2.** Microstructures of $LuBaCuFeO_5$ (a) and $TmBaCuFeO_5$ (b).

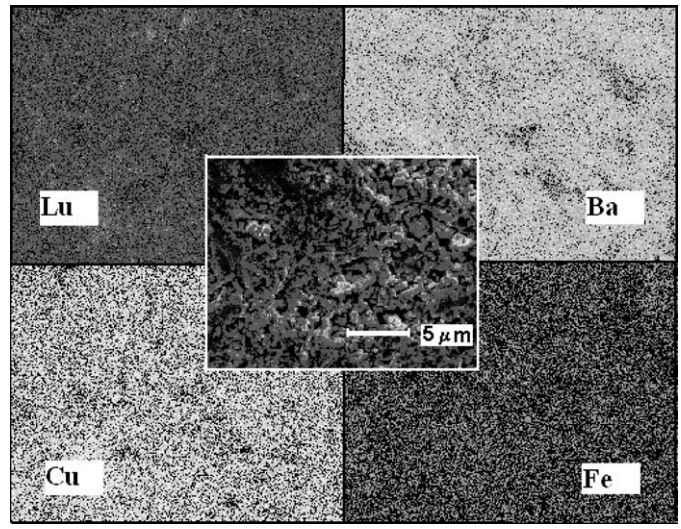


**FIG. 3.** Composition of images of EDS showing the distribution of Lu, Ba, Cu and Fe in the $LuBaCuFeO_{5+\delta}$ sample. The inner photograph shows the original region of the sample where EDS was performed.

agreement factors (in the *d*-spacing ranges 1.2–4 Å and 1.1–2.8 Å for LuBCFO and TmBCFO, respectively) using models (a) and (b) are showed in Table 1. In spite of the lower amount of variables refined using model (a), Hamilton's criterion (17) indicates that the improvement observed in the reliability factors is statistically significant. This structure is analogous with the one previously obtained for YBCFO (8). The oxygen atoms, both apical and equatorial, showed anisotropic vibrational behavior, but in contrast to other reports about YBCFO (7, 8), Fe and Cu also showed significant improvement when allowed to refine in anisotropic motion. The heavy rare-earth ions and barium display isotropic vibration. The occupancy of the apical oxygen atom has been refined and an extra oxygen with occupancy freely refined has been added, in the position to transform the pyramids in octahedra. The value of $\delta$ was determined to be 0.01(2) and $-0.02(2)$ for LuBCFO and TmBCFO, respectively.

As in other members of the *RE*BCFO series, the magnetic structure determination of LuBCFO and TmBCFO is led by the fact that the magnetic origin peaks indexed on the basis of the chemical unit cell as $(\frac{h}{2}, \frac{k}{2}, \frac{l}{2})$ with $h, k, l =$ odd. The most intense is the $(\frac{1}{2}, \frac{1}{2}, \frac{1}{2})_M$ peak located at $d \cong 5.1$ Å. With reference to the structural lattice constants the magnetic unit cell is then defined as $a_M = 2a$ and $c_M = 2c$ with a magnetic propagation vector $\mathbf{k} = (\frac{1}{2}, \frac{1}{2}, \frac{1}{2})$. The possible magnetic ordering schemes of both the $CuO_2$ and $FeO_2$ layers along the *c*-axis are $+[+-]-$ and $+[--]+$, where the bracket indicates the position of the rare earth ion (7, 8). The Rietveld profile refinements using the *d*-spacing range 3.1–7.9 Å established the best model as $+[--]+$ for both samples, with $R_{mag} = 12.6\%$ for LuBCFO at $T = 2$ K and 7.5% for TmBCFO at $T = 170$ K (lowest temperature available with enough *d*-spacing range to perform magnetic structure refinements). In this ordered model, the magnetic moments of the oxygen-sharing $Fe^{3+}$ and $Cu^{2+}$ ions point to the same

**TABLE 1**

**Reliability Factors from the Structural Refinements of $LuBaCuFeO_5$ and $TmBaCuFeO_5$ at 2 K, Using Models (a) Centrosymmetric Structure, 34 Variables Refined and (b) Non-Centrosymmetric Structure, 43 Variables Refined**

| | | $R_p$ (%) | $R_{wp}$ (%) | $\chi^2$ |
|---|---|---|---|---|
| $LuBaCuFeO_5$ | Model (a) | 9.61 | 8.13 | 9.5 |
| | Model (b) | 9.17 | 7.68 | 8.8 |
| $TmBaCuFeO_5$ | Model (a) | 7.01 | 6.42 | 6.7 |
| | Model (b) | 6.75 | 6.16 | 6.3 |

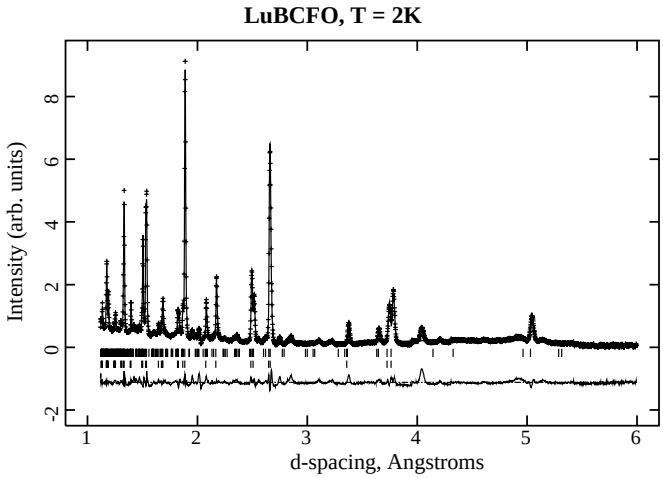


**FIG. 4.** Neutron powder diffraction profile of $LuBaCuFeO_{5+\delta}$ at $T = 2\,K$ and the Rietveld refinement, space group $P4\,mm$.Upper tick marks show the position for magnetic peaks (space group $P1$ was used in combination with suitable constraints) and lower tick marks the positions for nuclear peaks.

**TABLE 2**

**Final Structural Parameters Derived from the Rietveld refinements of $LuBaCuFeO_5$ at $T = 2\,K$ ($P4\,mm$ Space Group); $d$-Spacing Range: 1.2–4.0 Å**

| Atom | Site | $x/a$ | $y/b$ | $z/c$ | $U(\times 100)$ (Å$^2$) | Occup. |
|---|---|---|---|---|---|---|
| Lu | 1$a$ | 0 | 0 | 0.470(3) | 1.2(1) | 1 |
| Ba | 1$a$ | 0 | 0 | 0 | 2.3(2) | 1 |
| Cu | 1$b$ | $\frac{1}{2}$ | $\frac{1}{2}$ | 0.711(2) | $U11 = 5.1(2)$ | 1 |
| | | | | | $U33 = 0.8(7)$ | |
| Fe | 1$b$ | $\frac{1}{2}$ | $\frac{1}{2}$ | 0.257(2) | $U11 = 1.5(3)$ | 1 |
| | | | | | $U33 = 2.5(6)$ | |
| O1 | 1$b$ | $\frac{1}{2}$ | $\frac{1}{2}$ | 0.010(2) | $U11 = 0.8(3)$ | 0.98(2) |
| | | | | | $U33 = 7.8(6)$ | |
| O2 | 2$c$ | $\frac{1}{2}$ | 0 | 0.297(2) | $U11 = 3.9(5)$ | 1 |
| | | | | | $U22 = 0.7(5)$ | |
| | | | | | $U33 = 4(1)$ | |
| O3 | 2$c$ | $\frac{1}{2}$ | 0 | 0.657(2) | $U11 = 1.5(6)$ | 1 |
| | | | | | $U22 = 6.3(5)$ | |
| | | | | | $U33 = 0.8(5)$ | |

Lattice constants: $a = 3.774(1)$ Å, $c = 7.474(2)$ Å. Cell Volume = 106.45(5) Å$^3$; $R$-factors: $R_p = 9.17\%$, $R_{wp} = 7.68\%$, $\chi^2 = 8.8$.

direction. In the case of LuBCFO, the resulting magnetic moments associated with the $Fe^{3+}$ and $Cu^{2+}$ sublattices at $T = 2\,K$, are $\mu_{Fe} = 3.7(1)\,\mu_B$ and $\mu_{Cu} = 1.63(8)\,\mu_B$, respectively. According to these refinements the angles that the iron and copper magnetic moments form with the $c$-axis are 70(6) and 30(10)°, respectively. In TmBCFO the magnetic moments at $T = 170\,K$ for $Fe^{3+}$ and $Cu^{2+}$ sublattices are $\mu_{Fe} = 4.0(1)\,\mu_B$ and $\mu_{Cu} = 1.6(1)\,\mu_B$, respectively, and the angles that the iron and copper magnetic moments form with the $c$-axis are 75(7) and 10(3)°, respectively.

Figure 4 shows the structural and magnetic Rietveld refinement for LuBCFO at full $d$-spacing range, in space group $P4\,mm$, while the structural parameters for both samples, LuBCFO and TmBCFO, are detailed in Tables 2 and 3.

As previously observed in YBCFO (7–9), both LuBCFO and TmBCFO exhibit two peaks straddling the $(\frac{1}{2}, \frac{1}{2}, \frac{1}{2})$ magnetic peak, which is located at 5.051(3) and 5.062(3) Å. These satellites are named $(\frac{1}{2}, \frac{1}{2}, \frac{1}{2})^-$ and $(\frac{1}{2}, \frac{1}{2}, \frac{1}{2})^+$, located at lower and higher $d$-spacing, respectively. No comparable satellites could be detected surrounding any other magnetic peak. In YBCFO these peaks appear at temperatures below 190 K and the their magnetic nature was confirmed by polarization analysis (8). Due to the similarity of the shape and position of the satellites in LuBCFO or TmBCFO to those in YBCFO, they are assumed to be of magnetic nature as well. At 2 K the positions of the peaks in LuBCFO are 4.94(1) and 5.14(1) Å, and in TmBCFO are 4.94(1) and 5.15(1) Å, for $(\frac{1}{2}, \frac{1}{2}, \frac{1}{2})^-$ and $(\frac{1}{2}, \frac{1}{2}, \frac{1}{2})^+$, respectively. In both cases these peaks can be reasonably labeled as $(\frac{1}{2}, \frac{1}{2}, \frac{3}{8})$ and $(\frac{1}{2}, \frac{1}{2}, \frac{5}{8})$. The intensities of these peaks decrease with temperature as shown in Fig. 5, still remaining traces at the highest temperatures were recorded. This figure shows that, contrary to YBCFO (7, 8), the position of the satellites remains invariant in almost the whole range of temperature where data were collected (one previous report postulates the invariability of positions for YBCFO as well (9)).

The presence and positions of these peaks indicate the existence of a magnetic commensurate superstructure at

**TABLE 3**

**Final Structural Parameters Derived from the Rietveld Refinements of $TmBaCuFeO_5$ at $T = 2\,K$ ($P4\,mm$ Space Group); $d$-Spacing Range: 1.1–2.8 Å**

| Atom | Site | $x/a$ | $y/b$ | $z/c$ | $U(\times 100)$ (Å$^2$) | Occup. |
|---|---|---|---|---|---|---|
| Tm | 1$a$ | 0 | 0 | 0.475(4) | 1.9(1) | 1 |
| Ba | 1$a$ | 0 | 0 | 0 | 2.3(2) | 1 |
| Cu | 1$b$ | $\frac{1}{2}$ | $\frac{1}{2}$ | 0.701(2) | $U11 = 5.1(2)$ | 1 |
| | | | | | $U33 = 1.3(8)$ | |
| Fe | 1$b$ | $\frac{1}{2}$ | $\frac{1}{2}$ | 0.241(2) | $U11 = 1.2(4)$ | 1 |
| | | | | | $U33 = 0.7(6)$ | |
| O1 | 1$b$ | $\frac{1}{2}$ | $\frac{1}{2}$ | −0.005(4) | $U11 = 1.4(3)$ | 0.92(1) |
| | | | | | $U33 = 2.9(2)$ | |
| O2 | 2$c$ | $\frac{1}{2}$ | 0 | 0.296(2) | $U11 = 2.8(7)$ | 1 |
| | | | | | $U22 = 0.8(7)$ | |
| | | | | | $U33 = 0.6(1)$ | |
| O3 | 2$c$ | $\frac{1}{2}$ | 0 | 0.660(2) | $U11 = 0.2(1)$ | 1 |
| | | | | | $U22 = 4.3(6)$ | |
| | | | | | $U33 = 0.3(2)$ | |

Lattice constants: $a = 3.7812(2)$ Å, $c = 7.4854(4)$ Å. Cell volume = 107.02(1) Å$^3$ ; $R$-factors: $R_p = 6.75\%$, $R_{wp} = 6.16\%$, $\chi^2 = 6.3$.

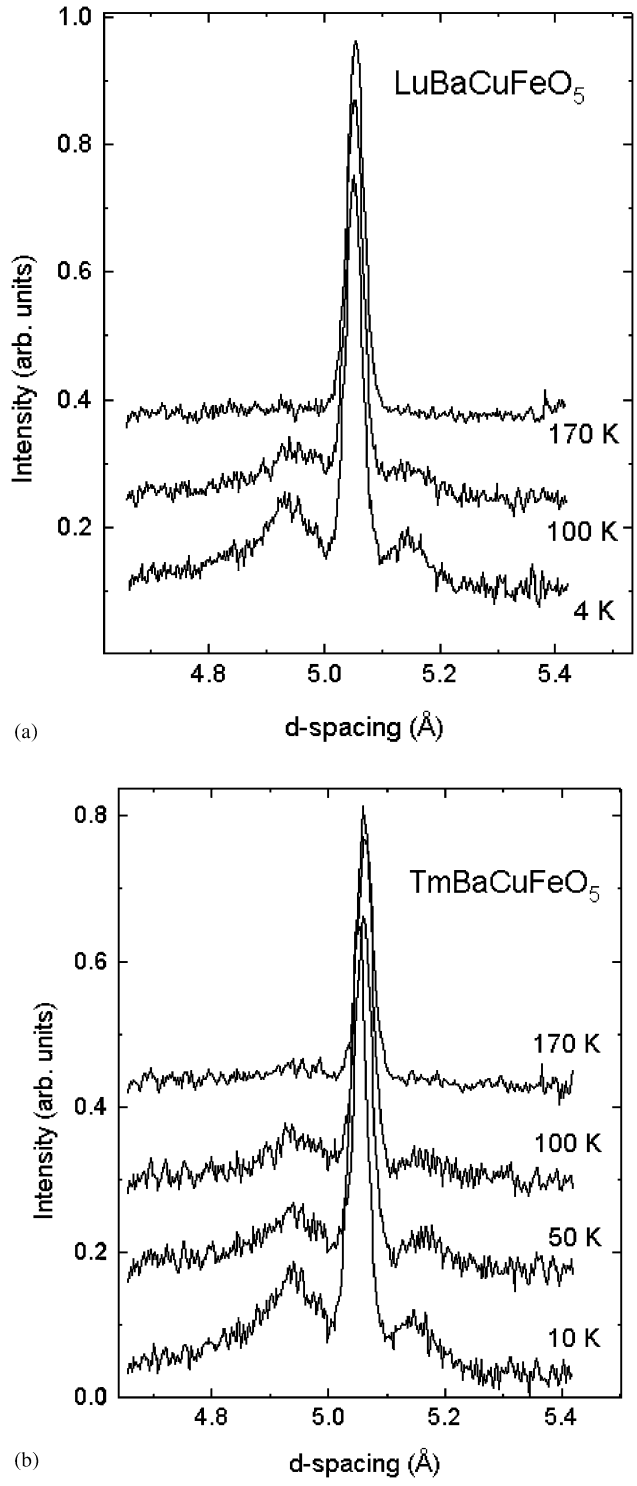


**FIG. 5.** Temperature evolution of the neutron diffraction profile of (a) $LuBaCuFeO_{5+\delta}$ and (b) $TmBaCuFeO_{5+\delta}$, in the vicinity of the $(\frac{1}{2}, \frac{1}{2}, \frac{1}{2})$ magnetic peak.

low temperatures in these systems. However, two different mechanisms can be invoked to explain the origin of this superstructure: a helimagnetic structure (8) and a model based on the existence of periodic reversing in the spin ordering in the spin sequence along one direction (9). The first structure supports a conical spin disposition where the helix angle is 135(2)°. The second structure can be schematized with the spin orientation of the $Cu^{2+}$ and $Fe^{3+}$ ions stacking along the *c*-axis shown in Fig. 6. Instead of exhibiting the simple antiferromagnetic ordering $+[--]+\,+[--]+\,+[--]+\,+[--]+\cdots$(Fig. 6(b)), this structure shows the ordering $+[--]+\,+[--]+-[++]--[++]-$, where $c_{\text{Mcomm.}} = 8c$ (Fig. 6(a)).

### 3.3. Magnetic Study

The temperature dependence of the DC-susceptibility in LuBCFO and TmBCFO with an applied field of 100 Oe, is shown in Fig. 7, where the zero field cooling (ZFC) and the field cooling (FC) branches can be seen. Both specimens show a clear and sharp transition at $T_1 = 14.0(5)$ K, previously reported by other authors to occur in YBCFO, but with no interpretation (3, 9). The LuBCFO specimen displays a second broad transition ($T_2$) in the region close to room temperature, indicated in the Fig. 8, that plots a wider temperature range at $H = 10$ Oe. Although this is not so evident for TmBCFO, the absence of a paramagnetic Curie-Weiss behavior suggests that there could be a second transition $T_2$ at temperatures higher than room temperature. It is quite evident that the LuBCFO exhibits a

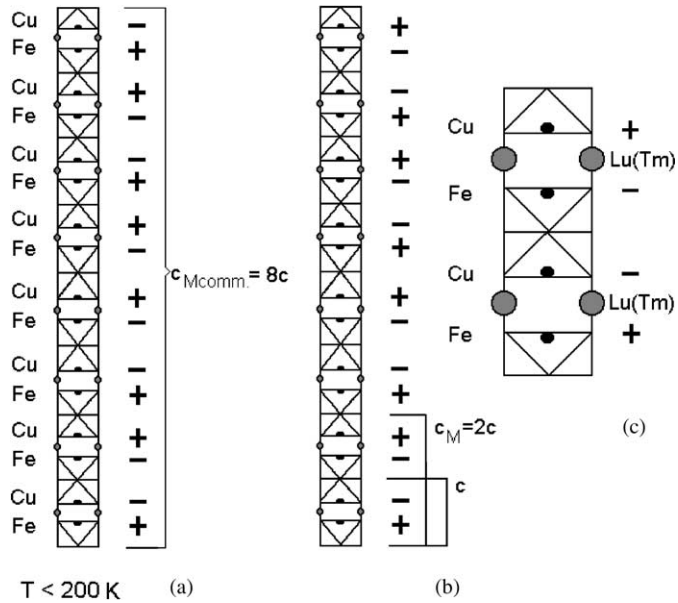


**FIG. 6.** Schematic representation of the spin sequences along the *c*-axis, where (a) the commensurate superstructure (with ordering $+[--]+\,+[--]+-[++]--[++]-$ and $c_{\text{Mcomm.}} = 8c$) and (b) the simple antiferromagnetic structure (exhibiting the simple antiferromagnetic ordering $+[--]+\,+[--]+\,+[--]+\,+[--]+$) are shown. (c) Exhibits the details of the simple antiferromagnetic unit cell.

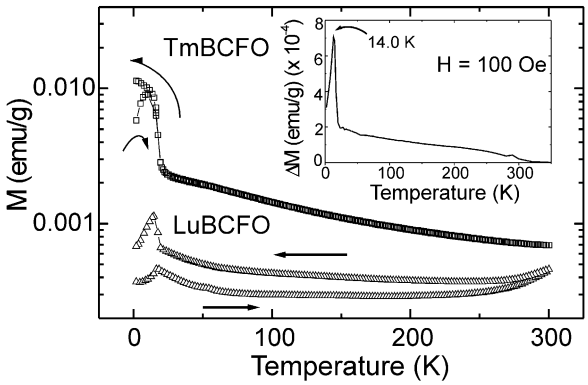


**FIG. 7.** Temperature dependence of the DC-susceptibility of $LuBaCuFeO_{5+\delta}$ and $TmBaCuFeO_{5+\delta}$, at $H = 100$ Oe. The arrows identify the ZFC and FC branches. The inset shows the difference between the ZFC and FC branches in $LuBaCuFeO_{5+\delta}$.

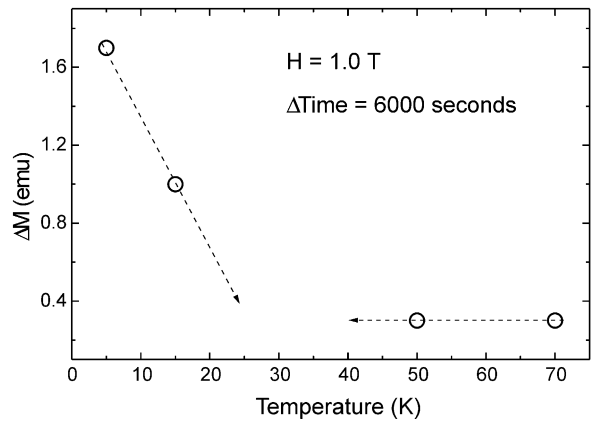


**FIG. 9.** Difference in the magnetization of $TmBaCuFeO_{5+\delta}$ when allowed to relax from $H = 1$ T for 300 s, during 6000 s.

very remarkable irreversible character up to almost room temperature. This irreversibility is enhanced below $T_1$ as it can be seen in the inset of Fig. 7, where the temperature dependence of the difference of the magnetization of both, the ZFC and the FC branches, is shown. The irreversibility in TmBCFO is almost negligible above $T_1$. The relaxation of the magnetization in these systems has been studied. Figure 9 shows the difference in the magnetization of TmBCFO when allowed to relax for 6000 s after applying a field $H = 1$ T for 300 s. It is possible to see that there is a trend to a sharp transition where the relaxation is more remarkable at temperatures below $T_1$.

## 4. DISCUSSION

As observed in YBCFO (8), the intensities of the satellites decrease when increasing temperature. In the literature there is an apparent disagreement about the reports of the transition temperature where the magnetic superstructure vanishes ($T_2$) for this phase. While this transition temperature according to neutron powder diffraction measurements is 190 K (8) (determined for the disappearing of the satellites), it is reported to be 230 K (7), 240 K (9) and 265 K (3), according to magnetic susceptibility results. This last work (3) reported the same transition temperature for samples prepared under different conditions (prepared under argon, air and oxygen). The difference between the temperatures reported by these groups confirms the broad character of the transition. The apparent disagreement between the transition temperature $T_2$ found using neutron powder diffraction data and magnetic measurement results is also observed in the present report for LuBCFO and TmBCFO, as well. Although this work does not present neutron powder diffraction measurements that exhibit the absence of satellites, it is evident that these peaks should disappear at temperatures not far from 200 K, as can be seen in Fig. 5. The temperature range where the magnetic measurements presented in this report does not allow to exactly determine the $T_2$ transition temperature for TmBCFO. However, a measurement with a wider temperature range showed that $T_2 = 303(3)$ K for LuBCFO. The reason for the apparent disagreement in the values of $T_2$ reported may be due to the different origins of the signals detected in each technique. Neutron powder diffraction requires coherence between the scattered waves originated at the crystalline planes. If these coherence weakens, then the intensity of the peaks will decrease. On the contrary, magnetic susceptibility measurements do not require that level of coherence, being able to detect signals from local ordering. This could be an explanation for the higher transition temperatures $T_2$ found using this kind of techniques. As seen in Fig. 5, the intensities of the satellites have already decreased at 170 K. An interpretation for this effect could be that at this temperature the stabilization of

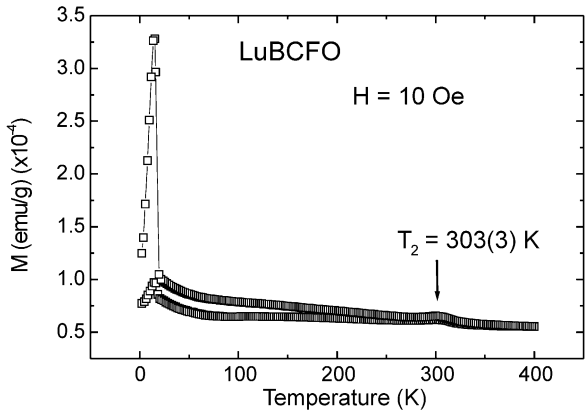


**FIG. 8.** Temperature dependence of the DC-susceptibility of $LuBaCuFeO_{5+\delta}$ at $H = 10$ Oe. The arrow indicates the temperature transition $T_2$.

the commensurate magnetic structure is decreased and a distribution of commensurate magnetic structures with different cells develops in the sample. Thus, at increasing temperatures the spin in some centers reverse and some different commensurate structures like $+[--]+ +[--]+-[++]--[++]-$, $+[--]+ +[--]+-[++]--[++]--[++]-$, $+[--]+ +[--]+ +[--]+-[++]--[++]--[++]-$ can coexist, leading to a rather diffuse scattering. Even it could be possible that at temperatures high enough a distribution of incommensurate magnetic structures could develop. In the case that a distribution of cells of commensurate magnetic structures with different sizes could coexist in the sample, these unit cells could not be strictly determined. Thus, the coherence required for a satellite peak to have non-negligible intensity could be much reduced. The same argument can be applied to a distribution of incommensurate magnetic structures. According to this explanation, the fact that these peaks disappear does not necessarily imply that no more magnetic superstructures are present in the sample, but rather they do not correspond to a unique ordering. This effect could be responsible for the apparent disagreement observed in the determination of $T_2$, since the magnetic measurements are not so dependent of a cooperative phenomenon. The broad transition observed for YBCFO (3, 7, 9) and LuBCFO (this report) could support this explanation. Figure 10 gives a schematic explanation of this effect using the collinear model already introduced in Fig. 6.

## 5. CONCLUSIONS

The studied samples, LuBCFO and TmBCFO, exhibit complex magnetic behaviors. They show a sharp transition associated with spin freezing at $T_1 = 14.0(5)\,\mathrm{K}$ where magnetization irreversibility is enhanced. While irreversibility in LuBCFO holds up to a second transition temperature in the proximity of room temperature, TmBCFO shows almost negligible irreversible behavior above $T_1$. The fact that the satellites surrounding the $(\frac{1}{2}, \frac{1}{2}, \frac{1}{2})$ magnetic peak only exhibit a minor smoothing when increasing temperature through $T_1$, suggests that the commensurate magnetic superstructure is independent of this irreversible behavior. The presence of the non-magnetic $Lu^{3+}$ in contrast to the magnetic $Tm^{3+}$ could be the key of the difference above $T_1$, since it allows a more diluted magnetic system. On the other hand, the irreversible behavior below $T_1$ is more intense for TmBCFO,

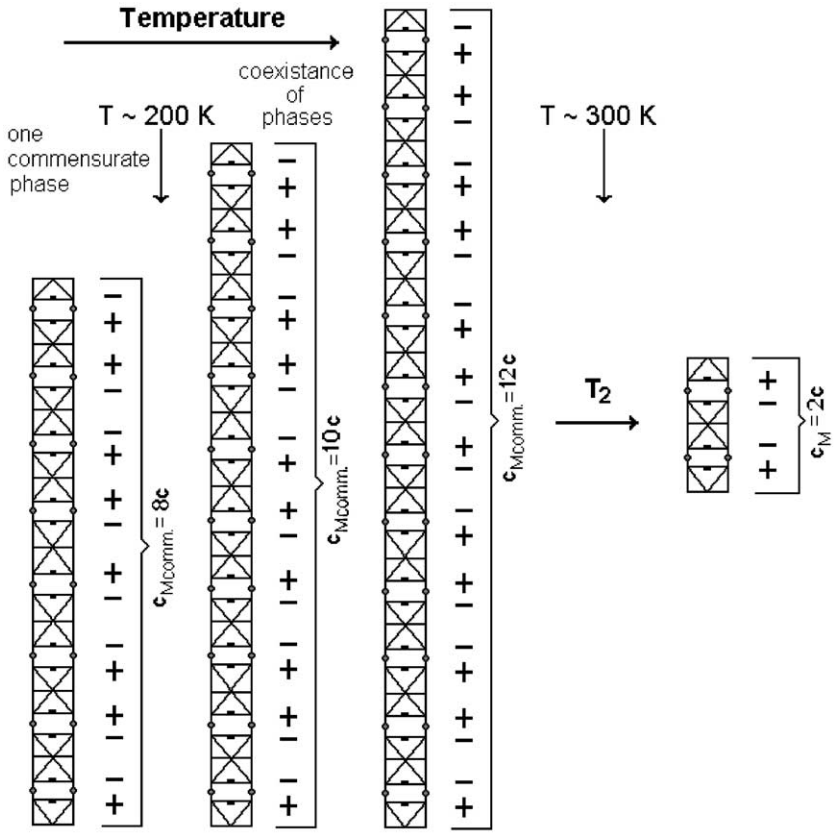


**FIG. 10.** Schematic representation of the possible spin sequences along the *c*-axis, where commensurate superstructures of different sizes are shown.

indicating that $Tm^{3+}$ magnetic centers participate in of the freezing.

In summary, the low-temperature magnetic behaviors in LuBCFO and TmBCFO, can be described as follows: a very intense spin freezing is observed below $T_1 = 14.0(5)$ K and a commensurate magnetic structure, present until temperatures close to 200 K. This structure evolves to a distribution of commensurate structures (even incommensurate magnetic structures could be present at temperatures high enough) that is present up to room temperature ($T_2 = 303(3)$ K, for LuBCFO). As in YBCFO (6–8), a simple antiferromagnetic structure is expected to exist above $T_2$.

## ACKNOWLEDGMENTS

The authors wish to thank PEDECIBA, CSIC and CONICYT (Uruguay), CNPq and FAPESP (Brazil) and EPSRC (UK) for financial support and the Rutherford-Appleton Laboratory, UK for provision of neutron time.

## REFERENCES

1. L. Er-Rakho, C. Michel, P. Lacorre, and B. Raveau, *J. Solid State Chem.* **73,** 521 (1988)
2. C. Meyer, F. Hartmann-Boutron, Y. Gros, and P. Strobel, *Solid State Commun.* **76,** 163 (1990)
3. M. Ruiz-Aragón, U. Amador, E. Morán, and N. H. Andersen, *Physica C* **1609,** 235–240 (1994)
4. Y. K. Atanassova, V. N. Popov, G. G. Bogachev, M. N. Iliev, C. Mitros, V. Psycharis, and M. Pissas, *Phys. Rev. B* **47,** 15201 (1993)
5. J. T. Vaughey and K. R. Poeppelmeier, "Proceedings of the International Electron Ceramics Conference, National Institute of Standards and Technology Special Publication, 804, p. 419." 1991.
6. A. W. Mombrú, C. Christides, A. Lappas, K. Prassides, M. Pissas, C. Mitros, and D. Niarchos, *Inorg. Chem.* **33,** 1255 (1994)
7. V. Caignaert, I. Mirebeau, F. Bourée, N. Nguyen, A. Ducouret, J. M. Greneche, and B. Raveau, *J. Solid State Chem.* **114,** 24 (1995)
8. A. W. Mombrú, K. Prassides, C. Christides, R. Erwin, M. Pissas, C. Mitros, and D. Niarchos, *J. Phys.: Condens. Matter* **10,** 1247 (1998)
9. M. J. Ruiz-Aragón, E. Morán, U. Amador, J. L. Martínez, N. H. Andersen, and H. Ehrenberg, *Phys. Rev. B* **58,** 6291 (1998)
10. M. J. Ruiz-Aragón, E. Morán, R. Sáez-Puche, N. Menéndez, and J. D. Tornero, *J. Superconductivity* **9,** 155 (1996)
11. M. Pissas, C. Mitros, G. Kallias, V. Psycharis, D. Niarchos, A. Simopoulos, A. Kostikas, C. Christides, and K. Prassides, *Physica C* **185,** 553 (1991)
12. M. Pissas, C. Mitros, G. Kallias, V. Psycharis, A. Simopoulos, A. Kostikas and D. Niarchos, *Physica C* **192,** 35 (1992)
13. M. Pissas, G. Kallias, V. Psycharis, H. Gamari-Seale, D. Niarchos and A. Simopoulos, *Phys. Rev. B* **55,** 397 (1997)
14. H. Pardo, W. A. Ortiz, F.M. Araújo-Moreira, L. Suescun, B. Toby, E. Quagliata, C.A. Negreira, K. Prassides, and A. W. Mombrú, *Physica C* **313,** 105 (1999)
15. A. W. Mombrú, H. Pardo, L. Suescun, B. H. Toby, W. A. Ortiz, C. A. Negreira, and F. M. Araújo-Moreira, *Physica C* **356,** 149 (2001).
16. A. C. Larson and R. B. Von Dreele, "Report No. LA-UR-86-748." Los Alamos National Laboratory, 1987.
17. W. C. Hamilton, *Acta Cryst.* **18,** 502 (1965)